



Submitted: 01-11-2019

Accepted: 08-12-2019

Pages:1-12

**SYNTHESIS OF CO₃O₄ NANOPARTICLES FROM AMINO ACIDS MIXED LIGANDS
AND ITS ADSORPTION PROPERTIES**

Farid I. El-Dossoki^{1,*}, Sarah. Rady², Nasser M. Hosny¹

¹ Chemistry Department, Faculty of Science, Port-Said University, Port-Said, Egypt

² Laboratory Specialist, Faculty of Pharmacy, Port-Said University, Port-Said, Egypt

*Corresponding author: Feldossoki64@sci.psu.edu.eg

ABSTRACT

The metal precursor derived from the reaction of Co(II) acetate with the mixed ligands of lysine(Lys) and glutamine(Glu) was used to synthesize Co₃O₄ nanoparticles. The precursor was characterized by (C, H, N, M), IR, electronic spectra, TGA and effective magnetic moments. Co₃O₄ nanoparticles were prepared from calcinations of the synthesized precursor at 800 °C. The obtained nanoparticles were characterized by X-ray powder diffraction and transmittance electron microscope. The average particle size is 50 nm. Co₃O₄ nanoparticles. Adsorption of Methylene Blue on the surface of the Co₃O₄ was studied. The synthesized metal oxide has 27.2 (mg/g) adsorption capacity of methylene blue (MB) from aqueous solution and removed 95 % of it. This method can be used to remove dyes from wastewater. Langmuir isotherm was the best model represents the adsorption of MB. Pseudo-second-order model with determination coefficient (R²) close to the unity was the best model for adsorption kinetic of MB.

Keywords:

Molecular precursors; Co₃O₄ nanoparticles; Adsorption.

1. INTRODUCTION

Lysine (Lys) is an amino acid involved polyamine synthesis, it is essential for the metabolic functions and animal growth [1]. The structures of amino acids can be affected by the interactions with neighbor amino acids or metal ions. Proton affinity (PA) is directly related to the stability of the zwitterion form of aliphatic amino acids [2-4]. These amino acids have proton affinities when bind to metal ions giving non Zwitter ionic structures [5, 6]. The physiological importance of glutamine (Gln) has been studied in the deamidation of

Gln [7-15]. Monitoring Gln deamidation is useful in study degradation effects on long-lived proteins characterized by slow turnover rates [12-16].

It is of considerable interest to use molecular precursor in synthesis of metal oxide nanoparticles. [17-25]. Using non-hydrolytic technique in preparations of metal oxide nanoparticles at high temperature can produce material with different properties [26].

Different methods as coagulation, ion exchange, flocculation, and other are used in the removal of heavy metals and dyes. There are some disadvantages of these methods as high cost, high sludge production, handling and disposal problems are presented. These disadvantages prompted searching for effective, low cost and environmentally save techniques for treatment of wastewaters. Adsorption of pollutants on low-cost adsorbents could be applicable and economically viable sustainable technology [27–31]. Metal oxide nanoparticles fit these criteria well. The existence of these materials in nanoscale provides high surface area and surface functional groups that can interact with dyes [32–36].

The present paper aims to synthesis of Co₃O₄ in nanoscale by environmentally safe techniques and to use it as adsorbent of methylene blue dye.

2. EXPERIMENTAL

2.1 Chemicals

Lysine and glutamine were purchased from Merck and cobalt acetate and methylene blue were purchased from ADWIC.

2.2 Apparatus and methods

Elemental Analysis was determined by using automatic (Elemental CHNS Analysis Analyser Vario–EL Model 111 Germany). Co(II) was determined by standard methods [37]. The electronic spectra of the precursor (in DMF) were measured on (JASCO Model V-630) UV2 Unicam UV/Vis. The effective magnetic moment was recorded on Sherwood scientific magnetic balance using the following equations:

$\chi_g = C l(R-R_0)/103m$; $\chi_m = \chi_g \cdot Mwt.10^{-3}$; $\mu_{eff} = 2.84 \sqrt{\chi_m T}$ (Where χ_g is the mass susceptibility per gm sample; C is the constant of the instrument; l is the sample length in cm; m is the weight of the sample; χ_g is the molar susceptibility, μ_{eff} is the effective magnetic moment and T is the absolute temperature). TGA measurement measured on (Disfrantial Thermal Analyser Thermo Gravimetric Analyser DTG 60 H). (FT/IR- 4100 type A) Mattson Spectrometer was used to measure IR spectra of the precursor in the range 400-4000 cm⁻¹ as KBr discs. XRD pattern was taken on Philips X PERT-PRO with nickel filtered Cu K α ($\lambda = 1.5405 \text{ \AA}$) radiation. CM 20 PHILIPS electron microscope was used to take TEM images.

2.3 Preparation of the precursor

The precursor was prepared by adding (0.2 gm) of the cobalt acetate in 20 ml distilled water to a mixture of (0.28 gm) of both lysine and of glutamine (0.14 gm) for each of the two amino acids in 30 ml distilled water. The mixture was refluxed for 4 hrs, then concentrated by evaporation at 50 oC. A precipitate is formed on addition of excess absolute ethanol. It was filtrated off, washed with ethanol and distilled water then, dried at 100 oC [38].

2.4 Synthesis of Co₃O₄ nanoparticles

1 gram of Co(II) precursor was ignited in a muffle furnace at 800 oC for 2 hrs in air. Co₃O₄ nanoparticles were obtained.

2.5. Adsorption of methylene blue

Methylene blue dye was removed by the prepared nanoparticles from aqueous solvent. Definite weight of Co₃O₄ oxide nanoparticles was put in definite volume of methylene blue aqueous solution of known concentration (10 ppm). The absorbance measured (at wavelength 664 nm) at different time intervals and at

pH nearly 7, using UV2 Unicam UV/Vis. Spectrometer. Adsorption capacity of MB in the surface of nanoparticles presented. The adsorption capacity (q_e) expressed in mg dye/g adsorbent and the (%) of dye removal determined at 25 °C at different time were calculated and presented.

3. RESULTS AND DISCUSSION

3.1 Elemental analysis

Co(II) precursor is violet in colour, soluble in water and organic solvents as DMF and DMSO. The elemental analysis is presented in (Table.1).

Table 1. Analytical data of Lys-Gln-metal complex Co(II)

Complex	Molecular Weight	color	M.P. °C	% Calculated				Found%			
				C	H	N	M	C	H	N	M
Co(Lys-Gln) ₂ .2H ₂ O	383.03	Violet	>300	34.7	6.7	14.6	14.3	35.0	6.4	13.7	13.7

3.2. Infrared spectra (FT-IR)

IR spectrum of lysine shows two bands around 3276 and 3040 cm⁻¹ was related to the asymmetric stretching vibrations of (NH₃⁺). Another bands at 1625 and 1605 cm⁻¹ were related to the asymmetric stretching vibrations of (COO⁻) and the in-plan-bending (NH₃⁺). The band at 1382 cm⁻¹ relates to the symmetric (COO⁻) [39].

There are several bands for glutamine appearing at 3408 and 3308 cm⁻¹ relate to the stretching vibrations of NH₂ group. The asymmetric and symmetric stretching vibrations of (COO⁻) appear at 1687 and 1586 cm⁻¹, respectively [40]. The band of (CO) appears at 1629 cm⁻¹.

Comparison the spectrum of the Co(II) precursor with the spectra of lysine and glutamine indicated blue shifts of the bands assigned to of (COO⁻) of lysine and glutamine, respectively. The difference between two the asymmetric and symmetric stretching vibrations is higher than 200 cm⁻¹, indicating the mono-dentate nature of the carboxylate group. The positions the bands attributed to amino groups were shifted after coordination to Co(II) ion (Table 2). From these observations it could be deduced that the amino acid coordinates to the metal ion in a bi-dentate manner through the carboxylate and amino groups (Fig.1.).

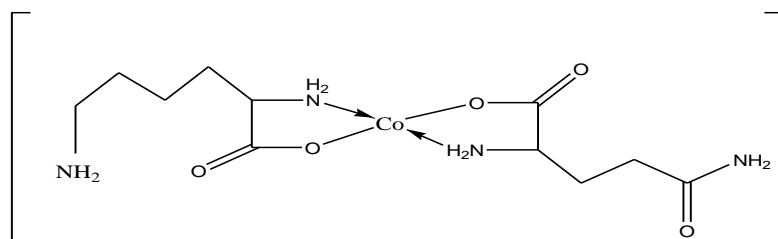


Fig. 1. Suggested structure of Co(II) precursor

The bands of vibration stretching of the terminal C=O in the spectra of the complexes remain approximately in their positions as an evidence of their inertness towards bonding to the metal ions. Many bands appear in the regions 565 and 490 cm⁻¹ due to $\nu(M-O)$ and $\nu(M-N)$ vibrations, respectively (Fig.2).

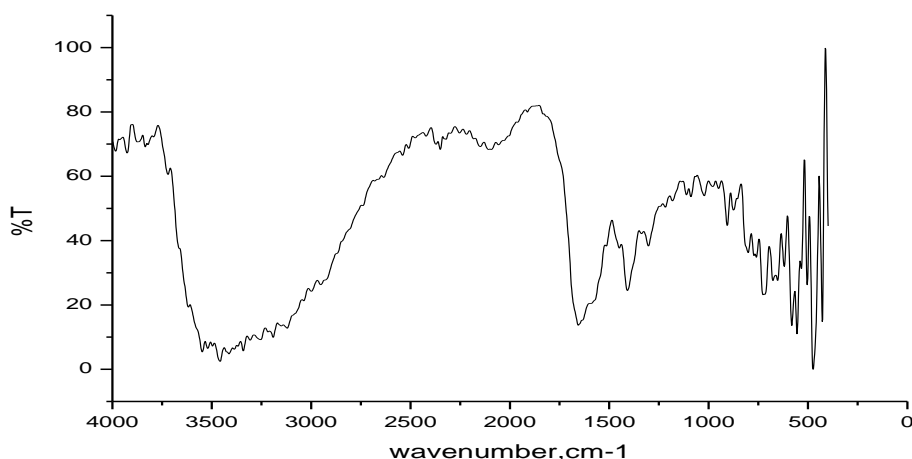


Fig. 2. IR spectrum of Co(II)-Lys-Gln complex

Table 2. Bands assignment of Lys, Gln and metal complex

assignment	Ligand (Lys + Gln)	Co complex
$\nu_{as}(\text{NH}_3^+)$	3276, 3040 3408, 3308	3232, 3169 3437, 3355
$\nu_{as}(\text{COO}^-)$	1625, 1687	1605, 1658
$\delta(\text{NH}_2^+)$	1497, 1605	1487, 1590
$\nu_s(\text{COO}^-)$	1382, 1586	1339, 1437
$\nu(\text{C}=\text{O})$	1629	1617
$\nu(\text{C}-\text{N})$	1410, 1004	1483, 962
$\rho(\text{NH}_2)$	810, 1052	837, 1001
(M-O)	—	565
(M-N)	—	490

3.3. Electronic spectra (UV/Vis)

Tetrahedral stereochemistry was suggested for Co(II) complex (Fig. 3) on the basis of the presence of a splitted band at 16583 cm^{-1} with a shoulder at 14880 cm^{-1} due to $4A_2 \rightarrow 4T_1$ transition, respectively [41]. The charge transfer band (LMCT) was observed at 25000 cm^{-1} . The value of magnetic moment (4.5 B.M.) agrees with the suggested stereochemistry.

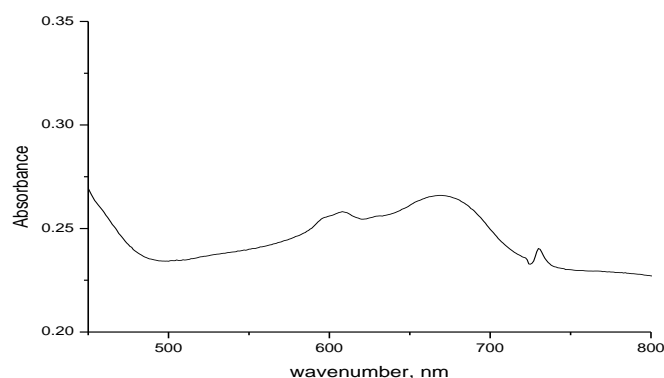


Fig. 3. Electronic spectra of Lys-Gln-Co(II) complex

3.4. Thermal analyses (TGA)

The thermal stability of Co(II) precursor was determined from thermal analyses. TGA-DTA curves of Co(II) precursor was represented in (Fig.4) and (Table 3).

Co(II) precursor decomposes in three steps, from 22 - 130 oC, 131 - 407 oC and 450 - 700 oC due to the elimination of two molecules of hydrated water, loss $C_6H_{10}N_2O_3$ and loss of $C_4H_{10}N$ respectively. With mass loss (Found Weight loss 9.1 %, Calculated Weight loss 9.3 %) for the first step, (Found Weight loss 40.5 %, Calculated Weight loss 41.2 %) for the second step and (Found Weight loss 22.6 %, Calculated Weight loss 22.1 %) for the third stage.

The thermodynamic parameters (E^* , ΔH^* , ΔG^* , ΔS^*) calculated by applying Coats- Redfern (CR) equation [42] and represented in (Table 4) and (Fig. 5).

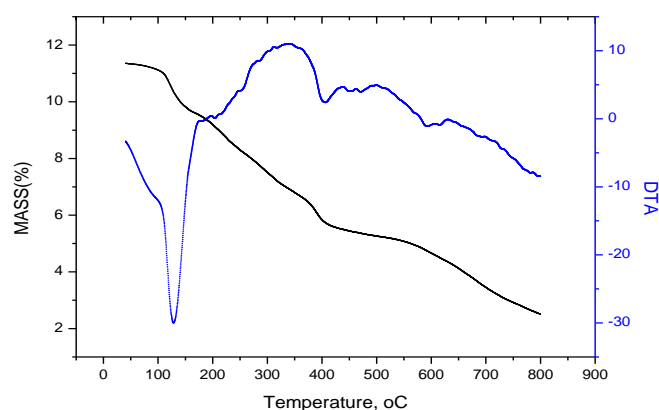


Fig. 4. TGA curves of Co(II) precursor

The high values of the activation energies (E) suggest that the aminoacid is strongly chelates Co(II) ion. The negative values of the entropy (ΔS^*) suggest that the activated has more ordered structure than the starting materials and the reactants are slower than the normal. The positive values of both the enthalpy (ΔH^*) and the free energy change (ΔG^*) confirm that the reaction is endothermic and nonspontaneous, respectively.

Table 3. Thermal analysis results of Lys-Gln-metal complex

Complexes	TGA steps	T, °C range	Wt. loss found (calculated)	Decomposed group
Co(II) complex	1	42 - 130	9.1 (9.3)	Loss of 2 H ₂ O
	2	131 - 407	40.5 (41.2)	Loss of C ₆ H ₁₀ N ₂ O ₃
	3	450 - 700	22.60 (22.10)	Loss of C ₄ H ₁₀ N

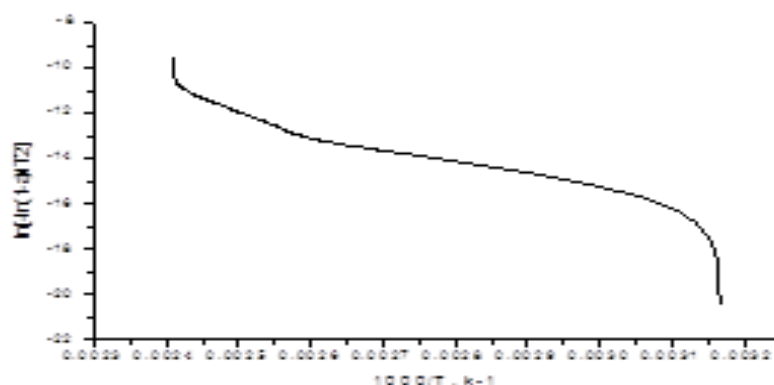


Fig. 5. Coats-Redfern relation for the main stage of the thermal decomposition of the precursor

Table 4. The thermodynamic parameters of decomposition of the Lys-Gln-metal complexes

Complex	TGA steps	E* kJ mol ⁻¹	¹ ΔS* kJ ⁻¹ mol ⁻¹	ΔH* kJ mol ⁻¹	ΔG* kJ mol ⁻¹
Co(II) precursor	1	1.00	-146.09	2.98	2.98
	2	1.32	-254.68	4.51	4.51
	3	9.44	-362.38	2.39	2.39
Total	—	11.76	-763.61	9.88	9.88

3.5. X-ray powder diffraction (XRD)

To insure the formation of cobalt oxid as a result of calcining the precursor X-ray diffraction was used. XRD pattern of ignition product of Co(II)precursor (Fig. 6) indicates the formation of Co₃O₄. The peaks at $2\theta = 31.21, 36.82, 38.51, 55.63, 59.27$ and 65.17 which are indexed to the planes (220), (311), (222), (400), (422), (511) and (411) of confirm the presence of pure Co₃O₄ nanoparticle (JCPDS 04-008-3173). The disappearance of any peaks due to other impurities insures the purity of this compound. From Debye Scherer formula, crystallite sizes determined from the major diffraction and found to be 50 nm Debye-Scherrer formula $D = 0.94 \lambda / \beta \cos\theta$ [43]. Where λ is the wavelength of x-ray (1.5406 Å) for Cu K α radiation, β is full width at half maximum and θ is the peak position. The particle size obtained by this method is smaller than that obtained from calcinations of cobalt salicylate precursor [44].

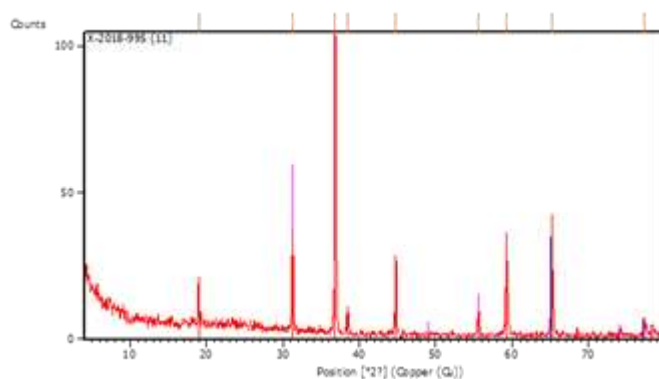


Fig.6. XRD pattern of Co₃O₄ nanoparticles

3.6. TEM

TEM images of Co₃O₄ nanoparticles indicated in (Fig. 7) crystalline product with average size 47-75 nm which lies in the same range as that calculated from XRD pattern.

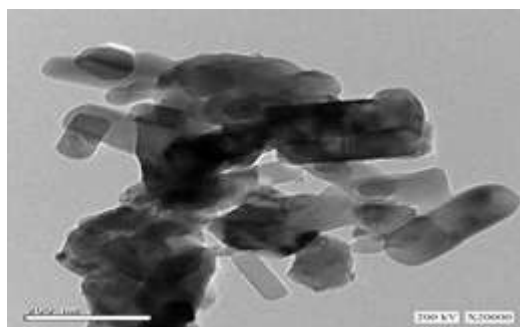


Fig. 7. TEM image of Co₃O₄ nanoparticles

3.7. Methylene Blue Adsorption

Organic dyes are an important part of many industrial effluents and require an efficient method of disposal. There are numerous conventional techniques of removing dyes including coagulation and flocculation, membrane filtration, oxidation or ozonation and precipitation. Activated carbon has been extensively used as an adsorbent in the removal of dye from waste water due to their microporous structure, large surface area and high sorption ability [45]. The previous techniques are expensive and large part of the cost is associated with high cost of maintaining the techniques and cost of chemicals. Hence, the use of indigenous techniques and locally sourced low-cost materials are imperative and seem to be the brightest solution to the ever increasing challenges of wastewater treatment. Adsorption process by molecules of gas, liquid, or dissolved solids added to a surface. This process creates a thin layer of the adsorbed material (atoms or molecules being adsorbed onto the surface of the adsorbing material. Just like surface tension, adsorption is as a result of surface energy [46].

Co₃O₄ used to remove MB from water. Adsorption capacity of MB in the surface of nanoparticles presented in (Fig. 8). The adsorption capacity (q_e) expressed in mg dye/g adsorbent and the (%) of dye removal determined at 25 °C at different time were presented in (Table 5). These data were obtained from equations (1) and (2) [47].

$$\% \text{ Dye Removal} = \left(\frac{C_0 - C_e}{C_0} \right) 100 \quad \text{----- (1)}$$

$$q_e = (C_o - C_e / m) V \quad \text{----- (2)}$$

(Co = the initial concentration in ppm of the adsorbate, and Ce = the equilibrium concentration in ppm, m = the weight of the adsorbent in (g), and V = the volume of the solution in (L). It is clear that, there is a direct relation between both (qe) and % of removal with the contact time. The rate of adsorption is high in the beginning of the adsorption process because of the presence of adequate surface area of the metal oxide nanoparticles available for adsorbing MB. This surface area is unavailable in the latter stages of adsorption process as the surface becomes saturated by MB.

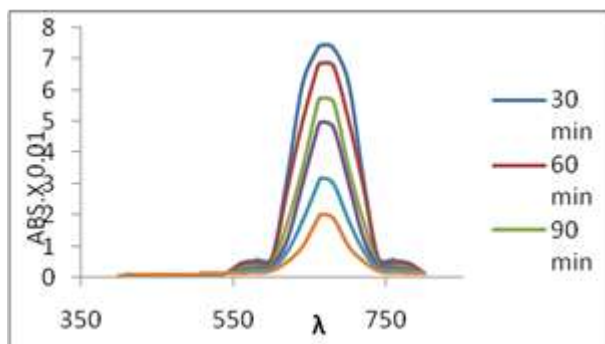


Fig. 8. Adsorption of MB on the Co3O4 nanoparticles at different times

Table 5. The adsorption capacity (qe) and the dye removal percentage at different time in at 25 °C

Time, Minute		30	60	90	120	150	180	q _{max}
Co ₃ O ₄	q _e , mg/g	26.1	26.2	26.4	26.6	27.0	27.2	27.2
	% Removal	91.4	91.8	92.6	93.4	94.7	95.5	

Langmuir isotherm equation (3) [48] applied to calculate the specific surface areas of nano-particles and the precursors.

$$S = (q_m \cdot a_{MB} \cdot N_A \cdot 10^{-23}) / M \quad \text{----- (3)}$$

S (10⁻³ km²/kg) = the specific surface area; q_m (mg/g) is the amount of MB adsorbed; the occupied surface area of one molecule MB (a_{MB}) = 197.2 Å² [49]; N_A (Avogadro’s number) = 6.02 x 10²³ mol⁻¹; M = the molecular weight of MB. From the results it is clear that, the specific surface area of Co₃O₄ is 86.36x10⁻³ km²/kg. The nanoparticles are higher than the values obtained for MB on the acid treated carbon (H₃PO₄-FAC with SMB; 18.170x10⁻³ km²/kg), the salt treated carbon, (ZnCl₂-FAC, SMB; 13.579 x10⁻³ km²/kg), the commercial carbon, CAC (SMB; 13.884x10⁻³ km²/kg) [50] and the activated carbon (21.06 x10⁻³ km²/Kg) [51].

3.8. Adsorption isotherms

By applying Langmuir [52], Freundlich [53] and Temkin [54] isotherm mode, Langmuir isotherm (Fig.9) was the best model represent the adsorption of MB. The correlation coefficient of R² value was close to unity. Q_{max} was calculated and collected in (Table 7). Langmuir adsorption isotherm was tested by applying the following equation:

$$(C_e/q_e) = (1/K_L \cdot q_m) + (C_e / q_m) \quad \text{----- (4)}$$

Where (q_m) is the maximum adsorption capacity expressed in mg dye/g adsorbent. Plotting of (C_e/q_e) versus C_e gives a straight line with slope = (1/q_m) and intercept = (1/K_L · C_e). From which the values of the maximum adsorption capacity (q_m) and Langmuir constant (K_L) were determined.

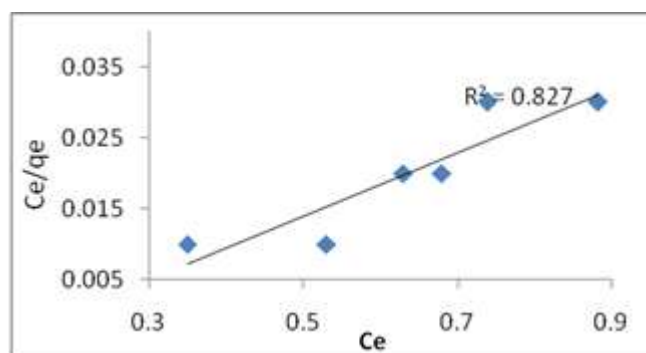


Fig. 9. Langmuir adsorption isotherm for Co₃O₄ nanoparticles

3.9. Kinetics Isotherms

Pseudo-first and second orders and intra-particle diffusion models [55] used to study the adsorption dynamics, but pseudo-second-order model with determination coefficient (R²) close to the unity (Fig. 10) and the other models showed small (R²) values. Pseudo-second-order model are expressed by the following equation:

$$(t/qt) = (1/k_2q_e) + t(1/q_e) \dots\dots\dots (5)$$

k₂ (g/ (mg•min)) is the pseudo-second-order rate constant. By plot (t/qt) versus t, k₂ and q_e were determined from the slope and intercept if value of q_e very close to experimental value then the reaction pseudo second order

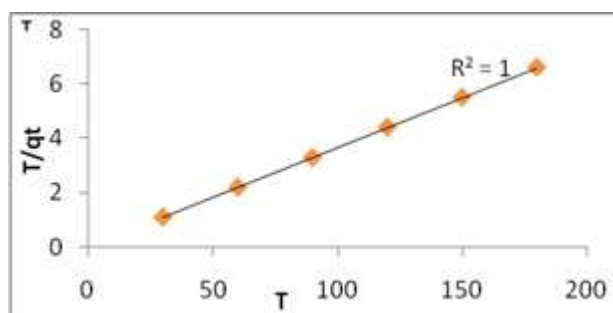


Fig. 10. Pseudo-second-order kinetic isotherm for Co₃O₄ nanoparticles

4. CONCLUSION

Molecule precursor derived from Co(II) with the mixed ligands lysine and glutamine was synthesized and characterized. Lysine and glutamine chelate Co(II) through carboxylate oxygen and amino nitrogen. The precursor was used to synthesize Co₃O₄ nanoparticles by thermal decomposition at 800 oC. The obtained nanoparticles were characterized by XRD and TEM. Adsorption of Methylene Blue on the surface of the Co₃O₄ was studied. The synthesized metal oxide has 27.2 (mg/g) adsorption capacity of methylene blue. This method can be used to remove dyes from wastewater.

REFERENCES

- [1] Yoshida, H. Nakano, Y. Koiso, K. Nohta, H. Ishida J. and Yamaguchi, M. Liquid chromatographic determination of ornithine and lysine based on intra-molecular excimer-forming fluorescence derivatization. *Anal. Sci.*, 17, 107-112, 2001.
- [2] Lemoff, A. S. Bush, M. F. Williams, E. R. Binding energies of water to sodiated valine and structural isomers in the gas phase: the effect of proton affinity on Zwitterion stability. *J. Am. Chem. Soc.*, 125, 13576-13584, 2003.
- [3] Wytttenbach, T. Witt, M. Bowers, M. T. On the stability of amino acid Zwitterions in the gas phase: the influence of derivatization, proton affinity, and alkali ion addition. *J. Am. Chem. Soc.*, 122, 3458-3464, 2000.
- [4] Hunter, E. P. Lias, S. G. In NIST Chemistry WebBook, NIST Standard Reference Database Number 69; Linstrom, P. J., Mallard, W. G., Eds.; National Institute of Standards and Technology: Gaithersburg, MD, 2003.
- [5] Talley, J. M. Cerda, B. A. Ohanessian, G. Wesdemiotis, C. Alkali metal ion binding to amino acids versus their methyl esters: affinity trends and structural changes in the gas phase. *Chem. Eur. J.*, 8, 1377-1388, 2002.
- [6] Jockusch, R. A. Price, W. D. Williams, E. R. L. Structure of cationized arginine ($\text{Arg}\cdot\text{M}^+$, $\text{M} = \text{H, Li, Na, K, Rb, and Cs}$) in the gas phase: further evidence for Zwitterionic arginine. *J. Phys. Chem. A* 103, 9266-9274 1999.
- [7] Robinson, N. E.; Robinson, A. B. Molecular clocks deamidation of asparaginyl and glutaminyl residues in peptides and proteins. Althouse Press: Cave Junction, OR, 2004.
- [8] Lindner, H.; Helliger, W. Age dependent deamidation of asparagine residues in proteins. *Exp. Gerontol.*, 36, 1551-1563, 2001.
- [9] Robinson, N. E.; Robinson, A. B. Deamidation of human proteins. *Proc. Natl. Acad. Sci. U. S. A.*, 98, 12409-12413, 2001.
- [10] Heaton, A. L.; Ye, S. J.; Armentrout, P. B. Experimental and theoretical studies of sodium cation complexes of the deamidation and dehydration products of asparagine, glutamine, aspartic acid, and glutamic acid. *J. Phys. Chem.*, 112, 3328-3338, 2008.
- [11] Heaton, A. L.; Armentrout, P. B. Experimental and theoretical studies of potassium cation interactions with the acidic amino acids and their amide derivatives. *J. Phys. Chem., B* 112, 12056-12065, 2008.
- [12] Wilson, J.; van Doorn, N. L.; Collins, M. J. Assessing the extent of bone degradation using glutamine deamidation in collagen. *Anal. Chem.*, 84, 9041-9048, 2012.
- [13] Robinson, N. E.; Robinson, A. B. Prediction of primary structure deamidation rates of asparaginyl and glutaminyl peptides through steric and catalytic effects. *J. Pept., Res.* 63(2004)437-448.
- [14] Robinson, N. E.; Robinson, A. B. Molecular Clocks. *Proc. Natl. Acad. Sci. U. S. A.*, 98, 944-949, 2001.
- [15] Li, X.; Lin, C.; O'Connor, P. B. Glutamine deamidation differentiation of glutamic acid and γ -Glutamic acid in peptides by electron capture dissociation. *Anal. Chem.*, 82, 3606-3615, 2010.
- [16] Catterall, J. B.; Hsueh, M. F.; Stabler, T. V.; McCudden, C. R.; Bolognesi, M.; Zura, R.; Jordan, J. M.; Renner, J. B.; Feng, S.; Kraus, V. B. Protein modification by deamidation indicates variations in joint extracellular matrix turnover. *J. Biol. Chem.*, 287, 4640-4651, 2012.
- [17] Murray, C. B.; Norris, D. J.; Bawendi, M. G. Synthesis and characterization of nearly mono-disperse CdE (E = sulfur, selenium, tellurium) semiconductor nanocrystallites. *J. Am. Chem. Soc.*, 115, 8706-8715, 1993.
- [18] Peng, X.; Wickham, J.; Alivisatos, A. P. Kinetics of II-VI and III-V Colloidal Semiconductor Nanocrystal Growth: "Focusing" of Size Distributions. *J. Am. Chem. Soc.*, 120, 5343-5344, 1998.

- [19] Sun, S.; Murray, C. Synthesis of mono-disperse cobalt nanocrystals and their assembly into magnetic superlattices (invited). *J. Appl. Phys.*, 85, 4325-4330, 1999.
- [20] JörgRockenberger, Erik C. Scher, A. Paul Alivisatos. A new non-hydrolytic single-precursor approach to surfactant-capped nanocrystals of transition metal oxides. *J. Am. Chem. Soc.*, 121, 11595-11596, 1999.
- [21] Brinker, C. J.; Scherer, G. W. *Sol-Gel Science*; Academic Press: San Diego, 1990.
- [22] Ziolo, R. F.; Giannelis, E. P.; Weinstein, B. A.; O'Horo, M. P.; Ganguly, B. N.; Mehrotra, V.; Russell, M. W.; Huffman, D. R. Matrix-mediated synthesis of nanocrystalline γ -Fe₂O₃: A new optically transparent magnetic material. *Science* 257, 219-223, 1992.
- [23] Matijevic, E. Preparation and properties of uniform size colloids. *Chem. Mater.*, 5, 412-426, 1993.
- [24] Moumen, N.; Pileni, M. P. New syntheses of cobalt ferrite particles in the range 2–5 nm: comparison of the magnetic properties of the nanosized particles in dispersed fluid or in powder form. *Chem. Mater.*, 8, 1128-1134, 1996.
- [25] Ying, J. Y. Special issue: sol-gel derived materials. *Chem. Mater.*, 9, 2247-2670, 1997.
- [26] Trentler, T. J.; Denler, T. E.; Bertone, J. F.; Agrawal, A.; Colvin, V. L. J. Am. Synthesis of TiO₂ nanocrystals by nonhydrolytic solution-based reactions. *Chem. Soc.*, 121, 1613-1614, 1999.
- [27] Chiron, N. Guilet, R. Deydier, E. Adsorption of Cu(II) and Pb(II) onto a grafted silica: isotherms and kinetic models. *Water Research.*, 37, 3079–3086, 2003.
- [28] Semerjian, L. Equilibrium and kinetics of cadmium adsorption from aqueous solutions using untreated Pinushalepensissawdust. *Journal of Hazardous Materials.*, 173, 236–242, 2010.
- [29] Ozacar, M. Sengil, A. Adsorption of reactive dyes on calcined alunite from aqueous solutions. *Journal of Hazardous Materials.*, 98, 221–224, 2003.
- [30] Debnath, S. Ghosh, U.C. Nanostructured hydrous titanium (IV) oxide: synthesis, characterization and Ni(II) adsorption behavior. *Chemical Engineering Journal.*, 152, 480–491, 2009.
- [31] Shi, K. Wang, X. Guo, Z. Wang, S. W. Se(IV) sorption on TiO₂: sorption kinetics and surface complexation modeling, *Colloids and Surfaces A. Physicochemical and Engineering Aspects.*, 349, 90–95, 2009.
- [32] Nano, G. V. Strathmann, T. J. Ferrous iron sorption by hydrous metal oxides. *Journal of Colloid and Interface Science.*, 297, 443–454, 2006.
- [33] O'Reilly, S. E. Hochella, M. F. Lead sorption efficiencies of natural and synthetic Mn and Fe-oxides. *Geochimica et Cosmochimica Acta.*, 67, 4471–4487, 2003.
- [34] Ada, K. Ergene, A. Tan, S. Yalcin, E. Adsorption of Remazol brilliant blue R using ZnO fine powder: equilibrium, kinetic and thermodynamic modeling studies. *Journal of Hazardous Materials.*, 165, 637–644, 2009.
- [35] Hashim, A. Thermodynamic study of adsorption Leshman's stain dye by germanium-oxide and yttrium-oxide. *European Journal of Social Sciences.*, 25, 364–371, 2011.
- [36] Hu, B.J. Zhong, L.S. Song, W.G. Wan L.J. Synthesis of hierarchically structured metal oxides and their application in heavy metal ion removal. *Advanced Materials.*, 20, 2977–2982, 2008.
- [37] Vogel A. I. "A Text Book of Quantitative Inorganic Analyses", 2nd Ed., Longman, London, 1961.
- [38] Tripathi, I. P. Kamal, A. Synthesis, characterization of some complexes of copper (II) with L-asparagine, L-histidine and L-lysine. *American Journal of Advanced Drug Delivery*, 3, 95-103, 2015.
- [39] Sung, Jang, D. Robert A. Condrate Sr. The I.R. spectra of lysine adsorbed on several cation-substituted montmorillonites. *Clays and Clay Minerals.*, 20, 79-82, 1972.
- [40] Dharmelincourt, P. Ramirez, F. J. Polarized micro-Raman and FT-IR spectra of L-Glutamine. *Appl. Spectrosc.*, 47, 446-451, 1993.
- [41] Lever, A. B. P. *Inorganic Electronic Spectroscopy*. Elsevier, Amsterdam, 1986.
- [42] Coats, A. W. Redfern, J. P. Kinetic. Parameter from thermogravimetric data. *Nature.*, 68, 201, 1964.

- [43] Klug, H. Alexander, L. "X-ray Diffraction Procedures", New York, Wiley; 1962.
- [44] Hosny, N. M. Single crystalline Co₃O₄ nanoparticles: Synthesis and optical properties. *J. Mat. Chem. Phys*, 144, 247, 2014.
- [45] Gopalakrishnan K, Manivannan, Jeyadoss. Comparative study on biosorption of Zn(II), Cu(II) and Cr (VI) from textile dye effluent using sawdust and neem leaves powder. *E-Journal of Chemistry*., 7, 504-510, (2010).
- [46] Nurul, S. A. Biosorption of methylene blue from aqueous solution using dried water hyacinth (*Eichornia crassipes*). *Journal of Environmental Resources*., 5, 67-74, 2009.
- [47] Forsner, U., Wittman, G. T., Metal pollution in the aquatic environment. 2nd edn Springer-Verlag, Berlin, Germany., 1981.
- [48] Itodo, A. U., Abdulrahman, F. W., Hassan, L. G., Maigandi, S. A., Itodo, H. U., Physicochemical parameters of adsorbents from locally sorted H₃PO₄ and ZnCl₂ modified Agricultural wastes, *New York Sci.*, 3(5), 17-24, 2010.
- [49] Graham, D. Characterization of physical adsorption systems. III. The separate effects of pore size and surface acidity upon the adsorbent capacities of activated carbons. *Phys. Chem.*, 59, 896-900, 1955.
- [50] Itodo, A. U., Itodo, H. U., Gafar, M. K. Estimation of specific surface area using Langmuir isotherm method. *J. Appl. Sci. Environ*, 144, 141-145, 2010.
- [51] Zheng, C., Zhou, X., Cao, H., Wang, G., and Liu, Z. Synthesis of porous graphene/activated carbon composite with high packing density and large specific surface area for supercapacitor electrode material. *Journal of Power Sources* 258, 290-296, 2014.
- [52] Langmuir, I. The adsorption of gases on plane surfaces of glass, mica and platinum. *J. Am. Chem. Soc.* 38, 2221-2295, 1916.
- [53] Freundlich, H. M. F., Over the Adsorption in Solution, *Physikalische Chemie (Leipzig)* 57, 385-471, 1906.
- [54] Temkin, M. I., Pyzhev, V. Kinetics of ammonia synthesis on promoted iron catalysts. *Acta. Physicochim URSS*, 12, 327-356, 1940.
- [55] Weber, W. J., and Morris, J. C. Kinetics of adsorption on carbon from solution. *Journal of the Sanitary Engineering Division*, 89, 31-60, 1963.